



1 **Holocene hydrological changes of the Rhone River (NW Mediterranean) as**
2 **recorded in the marine mud belt**

3 **Bassetti, M.A. (1), Berné S. (1), Sicre M.-A. (2), Dennielou B.(3), Alonso. Y. (1), Buscail R. (1),**
4 **Jalali, B. (4) ; Hebert B. (1), C. Menniti (1)**

5 (1) CEFREM UMR5110 CNRS, Université de Perpignan Via Domitia, France (2) Sorbonne Universités
6 (UPMC, Université Paris 06)-CNRS-IRD-MNHN, LOCEAN Laboratory, 4 place Jussieu, F-75005 Paris, France
7 (3) IFREMER, Centre de Brest, Plouzané, France (4) GEOGLOB, Université de Sfax, Tunisia.

8 **Abstract**

9 Expanded marine Holocene archives are relatively scarce in the Mediterranean Sea because most of the
10 sediments were trapped in catchment areas during this period. Mud belts are most suitable targets to access
11 expanded Holocene records. These sedimentary bodies represent excellent archives for the study of sea-land
12 interactions and notably the impact of the hydrological activity on sediment accumulation. We retrieved a 7.2 m-
13 long sediment core from the Rhone mud belt in the Gulf of Lions in an area where the average accumulation rate
14 is of ca. 0.70 m/1000 years. This core thus provides a continuous and high-resolution record of the last 10 ka cal
15 BP. A multi-proxy dataset (XRF-core scan, ¹⁴C dates, grain size and organic matter analysis) combined with
16 seismic stratigraphic analysis was used to document decadal to centennial changes of the Rhone hydrological
17 activity. Our results show that 1) the Early Holocene was characterized by high sediment delivery likely
18 indicative of local intense (but short duration) rainfall events , 2) important sediment delivery around 7 ka cal BP
19 roughly presumably related to increased river flux, 3) a progressive increase of continental/marine input during
20 the Mid-Holocene despite increased distance from river outlets due to sea-level rise possibly related to higher
21 atmospheric humidity caused by the southward migration of the storm tracks in the North Atlantic, 4) multi-
22 decadal to centennial humid events in the Late Holocene. Some of these events correspond to the cold periods
23 identified in the North Atlantic (Little Ice Age, LIA; Dark Age) and also coincide with time intervals of major
24 floods a in the Northern Alps. Other humid events are also observed during relatively warm periods (Roman
25 Humid Period and Medieval Climate Anomaly).

26 **1. Introduction**

27 The Holocene climate is characterized by centennial-scale climate changes that punctuated the
28 final deglacial warming after the Younger Dryas (Ishihama et al., 2014; Ishihama et al.;
29 Renssen et al., 2009; Rogerson et al., 2011; 2004; Wanner et al., 2008). Wanner et al. (2014)
30 provided an extensive review of Holocene climate variability mainly based on
31 chronologically well-constrained continental temperature time series that emphasize the
32 superimposition of the insolation-driven climate changes with those induced by other external
33 forcings such as solar activity, volcanism and greenhouse gases (CH₄, CO₂ and NO₂). Based
34 on existing data, Holocene climate can be divided into four periods:



35 a) the early Holocene (between 11.7 and 8.2 ka cal BP, Walker et al., 2012) characterized by a
36 progressive warming inducing ice-cap melting and outbreaks of freshwater from North
37 America glacial lakes leading to a regional cooling in the Northern Hemisphere, *i.e.* the 8.2 ka
38 cal BP cold event (Barber et al., 1999);

39 b) the warm middle Holocene (between 8.2 and 4.2 ka cal BP, Walker et al., 2012) that
40 coincides approximately with the Holocene Thermal Maximum (HTM) and is punctuated by
41 several cold relapses (CR) (Wanner et al., 2011). Events at 6.4, 5.3 and 4.2 ka cal BP are the
42 most significant in terms of temperature change (Wanner et al., 2011). The 4.2-ka event
43 corresponds to enhanced dryness in the Southern Mediterranean, Asia and North America,
44 that may have presumably played a role in the collapse of various civilizations (Cronin et al.,
45 2013; Magny et al., 2013).

46 c) the cold late Holocene (from 4.2 ka cal BP to the mid 19th century, Walker et al., 2012) that
47 includes the 2.8 ka cal BP cold event possibly responsible for the collapse of the Late Bronze
48 Age civilization (Do Carmo and Sanguinetti, 1999; Weiss, 1982) and the Migration Period
49 cooling around 1.4 ka cal BP (Wanner et al., 2014). The late Holocene cooling trend
50 culminated during the Little Ice Age (LIA) between the 13th and 19th century (Frezza and
51 Carboni, 2009);

52 d) the warm Industrial Era from 1850 AD onwards (Cronin et al., 2002; Rogerson et al., 2011;
53 Wanner et al., 2011).

54 In contrast to these cool events, the Medieval Climate Anomaly (MCA, 800-1300 AD) is
55 often described as a warm period characterized by intense dryness in some regions of the
56 Northern Hemisphere, such as for example Europe and the Mediterranean region (Cronin and
57 Raymo, 1997) although not synchronous worldwide (PAGES 2k Consortium, 2013).

58 The causes of Holocene climate variability are not yet fully understood despite recent
59 advances achieved through the study of climate archives from all around the world from both
60 marine and continental settings. To what extent these well-known climate events are global
61 rather than regional and what are the driving mechanisms at play are still open questions.
62 Numerical modelling allows examining in more details and on a broader geographical scale
63 causes of rapid climate changes and the role of natural or anthropogenic forcings by better
64 integrating data from marine, land and ice archives (Fontanier et al., 2005; Fontanier et al.,
65 2006; Müller and Suess, 1979; Perez-Sanz et al., 2014; Puig et al., 2004; Schmiedl et al.,
66 2004; Van der Zwaan et al., 1999). Nonetheless, there are significant discrepancies between
67 proxy reconstructions and numerical simulations that suggest the need to generate better
68 chronologically constrained high-resolution proxy records from continental and marine



69 archives and develop new approaches (Anchukaitis and Tierney, 2013; Evans et al., 2013). Of
70 particular interest are the locations that allow developing paleo-hydrological and paleo-
71 environmental investigations at the land / sea interface to better link atmospheric circulation
72 controlling the precipitation pattern over the continent and changes in the thermohaline
73 circulation. Sediment drifts fed by water streams connected to the deep sea such as the Var
74 (Bonneau et al., 2014) or mid-shelf mud belts are interesting locations to recover sedimentary
75 archives where both continental and marine proxies can be analyzed. Mid-shelf mud belts, in
76 particular, are depot centers fed by streams that result from various processes including
77 diffusion under the influence of storms, advection by currents and transport by gravity flows
78 (Hill et al., 2007). They often form elongated sediment bodies, between 10-30 m and 60-
79 100 m water depth, roughly parallel to the coastline. Such sediment bodies can reach several
80 10th of meters thickness when they are associated to large streams, and form infralittoral
81 prograding prisms (sometimes called subaqueous deltas) as for instance along the Italian
82 Adriatic coast (Cattaneo et al., 2003). Somehow, they are shallow-water equivalents to
83 contourites, but they generally display higher accumulation rates making them ideal targets
84 for paleo-environmental reconstructions.

85 In this study, we present a continuous record of the Holocene climate obtained from a 7.2 m-
86 long sediment core retrieved from the Rhone mud belt in the Gulf of Lions. Owing to the high
87 sedimentation rate of this environmental setting, we could generate sedimentological data at
88 decadal scale resolution for sediment grain size and semi-quantitative chemical composition
89 obtained by mean of continuous X-ray fluorescence. Organic matter parameters and the
90 overall seismic architecture of the mud-belt were also used to reconstruct the terrigenous flux
91 and the degree of alteration of land-derived material for investigating the relationship between
92 detritic fluxes and the paleohydrology of peri-Mediterranean rivers. Based on the comparison
93 of available data, we explored the linkages between rapid climate changes and continental
94 paleo-hydrology with a focus on the Rhone river flood activity.

95

96 **2. Environmental and climatic framework**

97 **2.1. The Gulf of Lions geological and oceanographic settings**

98 The Gulf of Lions (GoL) is a passive and prograding continental margin with a relatively
99 constant subsidence and a high sediment supply (Berné and Gorini, 2005). Located in the
100 north-west sector of the Mediterranean Sea, the GoL is bounded to the West and to the East



101 by the Pyrenean and Alpine orogenic belts, and comprises a crescent-shaped continental shelf
102 with maximum width of 72 km near the mouth of Rhone (Berné et al., 2004). The general
103 oceanic circulation is dominated by the geostrophic Liguro-Provençal or Northern Current
104 (Millot, 1990), which is the northern branch of the general cyclonic circulation in the western
105 Mediterranean basin. This current flows southwestward along the continental slope and
106 temporally intrudes on the continental shelf during northwesterly winds events (Millot, 1990;
107 Petrenko, 2003). Surface water circulation in the GoL shelf is wind-dependent (Millot, 1990).
108 Different wind patterns affect the circulation and transport of suspended particles on the shelf
109 and produce distinctive wave regimes. The continental cold and dry winds known as the
110 *Mistral* and *Tramontane*, blowing from the N and NW through the passages between the
111 Pyrenees, Massif Central and the Alps, are associated with a short fetch that generate small
112 waves on the inner shelf. During winter, these winds induce strong cooling and mixing of the
113 shelf-waters triggering dense water formation (Estournel et al., 2003) and locally generating
114 upwelling (Millot, 1990). Episodic and brief E-SE (*Marin* or Maritime regime) winds are
115 associated with long fetch and large swells. This wind regime induces a rise in sea level along
116 the shore and intense cyclonic circulation on the shelf (Ulses et al., 2008) producing
117 alongshore currents and down-welling (Monaco et al., 1990). Transport of humid marine air
118 masses over the coastal relief induces abundant precipitations often accompanied by river
119 flooding.

120 The main source of sediment in the GoL is the Rhône River (Pont et al., 2002) and to a lesser
121 extent, small rivers of the Languedoc-Roussillon region (Hérault, Orb, Aude, Agly, Têt, Tech)
122 (Figure 1). The latter experience episodic discharges (*flash floods* in spring and fall) that are
123 difficult to quantify. The terrigenous sediment supply originating from the Rhone River
124 represents 80% of the total sediment deposited on the shelf (Aloisi et al., 1977). The Rhone
125 River drains a largely mountainous catchment area of 97 800 km² incising a geologically
126 heterogeneous substrate, consisting of siliciclastic and carbonate sedimentary rocks in valley
127 infills and a crystalline (plutonic and metamorphic from the Alpine domain) bedrock. The
128 mean annual water discharge measured at Beaucaire gauging station, downstream the last
129 confluence is 1,701 m³ s⁻¹ (mean for 1961-1996) ; the solid discharge varies between 2 to 20
130 10⁶ tons yr⁻¹ (Eyrolle et al., 2012; Pont et al., 2002).

131 Most of the sediment delivered by the Rhone is trapped on the inner shelf mainly in prodeltas
132 (Fanget et al., 2013; Ulses et al., 2008) but redistribution processes operating along the shelf
133 create mid-shelf depocenters of fine sediments. The sediment accumulation rate varies from



134 20 to 50 cm yr⁻¹ at the present Roustan mouth of the Rhone River and strongly decreases with
135 the distance from the river. Sediment is exported seaward by several turbid layers: the surface
136 nepheloid layer, related to river plume; an intermediate nepheloid layer that forms during
137 periods of water-column stratification; and a persistent bottom nepheloid layer whose
138 influence decreases from the river mouth to the outer shelf (Calmet and Fernandez, 1990;
139 Naudin et al., 1997). The surficial plume is typically a few meter-thick close to the mouth but
140 rapidly thins seaward to few centimeters (Millot, 1990); it is deflected southwestward by the
141 surface water circulation on the GoL shelf. The predominance of the Rhone River in the
142 sediment supply and the continental shelf circulation allow the identification of several zones
143 in the GoL (Durrieu De Madron et al., 2000): i) the deltaic and prodeltaic sediment units
144 where most of the sediments are trapped, ii) the mid-shelf mud belt between 20 and 50-90 m
145 depth resulting from sediment transport under the influence of the main cyclonic westward
146 circulation and iii) the outer shelf where fine-grained sedimentation is presently very low and
147 where relict fine sands are episodically reworked during extreme meteorological events
148 (Bassetti et al., 2006).

149 **2.2. Holocene paleohydrology in the western Mediterranean**

150 The Mediterranean hydrology is controlled by the seasonality of precipitation as well as the
151 catchment geology, vegetation type and geomorphology of the region. In northwestern
152 Mediterranean the most important fluvial discharges occur in spring and autumn, while
153 minimum flow is observed in summer (Thornes et al., 2009). On Holocene time scale, the
154 Mediterranean fluvial hydrology is characterized by the alternation of wet and dry episodes
155 related to changes in atmospheric circulation leading to a North-South hydrological contrast
156 in the Mediterranean region with climate reversal occurring at about 40°N (Magny et al.,
157 2013). Complex climate regimes result from external forcings (orbital, solar activity,
158 volcanism) as well as from internal modes of atmospheric variability such as the North
159 Atlantic Oscillation, East Atlantic, East-Atlantic-West Russian or Scandinavian modes (Josey
160 et al., 2011; Magny et al., 2013).

161 In the NW Mediterranean, the Holocene fluvial hydrology has been reconstructed using major
162 hydrological events (extreme floods and lake levels) recorded in lake and fluvial sediments
163 (Arnaud et al., 2012; Benito et al., 2015; Magny et al., 2013; Wirth et al., 2013). Overall, the
164 early Holocene climate was generally dry except for short pulses of higher fluvial activity
165 reported in the Durance and southern Alps rivers (Arnaud-Fassetta et al., 2010). A marked
166 cooling trend is observed with a major change around 7,500 a cal BP (Fletcher and Sánchez



167 Goñi, 2008) corresponding to humid conditions in the Iberian peninsula (Benito et al., 2015).
168 The mid-Holocene (from ca. 7,000 to 5,000 a cal BP) also records low torrential activity but
169 increasing flood frequency between 6,000 and 4,500 a cal BP in Spain, Tunisia and southern
170 France (Arnaud-Fassetta, 2004; Benito et al., 2003; Faust et al., 2004) that evolves in the late
171 Holocene to a general increase of fluvial activity, at least in the Rhone basin catchment and
172 north Alps domain (Wirth et al., 2013). In addition, anthropogenic activities (agriculture and
173 deforestation) over the last 5,000 years have modified the erosional rate in the catchment area,
174 resulting in increased/decreased sediment delivery to the sea depending on the
175 deforestation/forestation phases related to the agricultural development (Arnaud-Fassetta et
176 al., 2000; van der Leeuw, 2005).

177 **2.3. Deglacial and Holocene history of the Rhone Delta**

178 During the last ca. 20 ka, the morphology of the Rhone delta strongly evolved in response to
179 sea-level and climate changes. At the end of the Last Glacial Maximum, the Rhone reached
180 the shelf edge and directly fed the Petit Rhone Canyon (Figure 1) (Lombo Tombo et al.,
181 2015). The disconnection between the river and the canyon head is dated at 19 ka cal BP in
182 response to the acceleration of sea-level rise (*ibid.*). The retreat path of the estuary mouth on
183 the submerged shelf has been tracked through the mapping and dating of paleo-deltas (Berné et
184 al., 2007; Fanget et al., 2014; Gensous and Tesson, 2003; Jouet, 2007; Lombo Tombo et al.,
185 2015) and, onshore, through the study of ancestral beach ridges (Arnaud-Fassetta, 1998;
186 L'Homer et al., 1981; Vella and Provansal, 2000). During the Younger Dryas, an “Early
187 Rhone Deltaic Complex” (ERDC) formed at depths comprised between -50 and -40 m below
188 present sea level (Berné et al., 2007). The estuary then shifted to the NW as sea-level rose
189 during the Early Holocene (Fanget et al., 2014). The period of maximum flooding in the delta
190 (the turnaround between coastal retrogradation and coastal progradation) is dated at ca. 8,500
191 -7,500 a cal BP (Arnaud-Fassetta, 1998). Around this time, the mouth of the Rhone was
192 situated about 15 km North of its present position. Between this period and the Roman Age
193 (approximately 20 BC-390 AD in Western Europe), the position of the Rhone outlet(s) are not
194 precisely known and many distributaries, with their associated deltaic lobes, have been
195 identified. However, there is a general consensus on the eastward migration of the delta from
196 the St Ferreol Distributary that occupied the position of the modern Petit Rhone between ca.
197 6,000 and 2,500 a cal BP, and the modern Grand Rhone, built at the end of the 19th century.
198 To the West of the Rhone, a mud belt/subaqueous delta, about 150 km in length, up to 20 m



199 thick, is observed (Figure 1). So far, little attention has been paid to this sediment body, and
200 neither seismic data nor detailed core analysis were available.

201

202 **3. Material and methods**

203 The gravity core KSGC-31 was retrieved from the Rhone mud belt (43°0'23''N; 3°17'56''E,
204 water depth 60 m) during the GM02-Carnac cruise in 2002 on the R/V "Le Suroît". Seismic
205 data were acquired in 2015 aboard R/V Néréis during the Madho1 cruise, using an SIGTM
206 sparker. The shooting rate was 1s. Data were loaded on a KingdomTM workstation. An
207 average seismic velocity of 1,550 ms⁻¹ (based on measurements of sonic velocity with a
208 GeotekTM core logger) was used to position the core data on seismic profiles. The uncertainty
209 in the position of time lines on the seismic profile at the core position is on the order of ±
210 0.5 m, taking into account the resolution of the seismic source, the errors in positioning and
211 sound velocity calculation. Due to the shallow water depth, core deformation by cable
212 stretching is considered as negligible.

213 Grain size analyses were carried out by mean of a MalvernTM Mastersize 3000 laser
214 diffraction particle size analyzer using a HydroEV dispersing module, which measures
215 particle grain-sizes between 0.04 and 3,000 µm. Samples were dispersed in a solution of
216 (NaPO₃)₆ (1.5 gr/l of distilled water) for 1 hour in order to better disaggregate the sediment.
217 Before each measurement, the sample was stirred on a rotating mixer during 20 minutes.
218 Grain-size parameters were measured all along the core every cm. Three size ranges were
219 used to classify the grains: clay (<8 µm, as recommended by Konert and Vandenberghe
220 (1997), coarse silt (>8 µm and <63 µm), sand (>63 µm and < 250 µm). The D50, representing
221 the maximum diameter of 50% of the sediment sample was calculated.

222 Core KSGC31 was analyzed using an Avaatech XRF Core Scanner at IFREMER (Brest,
223 France). This non-destructive method provides semi-quantitative analyses of major and minor
224 elements by scanning split sediment cores (Richter et al., 2006). Measurements were
225 performed every 1 cm with a counting time of 20 sec and a 10kV and 30kV acceleration
226 intensity. Resulting element abundances are expressed as element-to-element ratio. Three
227 ratios are used in this work: 1) **Ca/Ti** ratio, to account for two end-members in the sediment
228 composition. The Ca is supposedly mostly derived from biogenic carbonates, while Ti is
229 commonly used for tracking terrigenous sediments, even if usually found in small amounts.
230 Nonetheless, it is worthwhile reminding that calcite of detritic origin might be important in



231 the fluvial Rhône waters but this kind of CaCO_3 is mainly accumulated in the sand fraction
232 and quickly decreases seaward of the river mouth (Chamley, 1971). A small fraction of
233 detritic calcite can be preserved in the clay fraction but represents a minor component; 2)
234 **Zr/Rb** reflects changes in grain size, with higher values in the relatively coarse grained
235 sediments. Zr is enriched in heavy minerals and commonly associated with the relatively
236 coarse-grained fraction of fine-grained sediments (highest Zr values are found in sandstones),
237 whereas Rb is associated with fine-grained fraction, including clay minerals and micas
238 (Dypvik and Harris, 2001) ; 3) **K/Ti** values can be related to illite content. Illite is formed by
239 weathering of K-feldspars under subaerial conditions and most of the K leached from the
240 rocks is adsorbed by the clay minerals and organic material before it reaches the ocean
241 (Weaver, 1967). In the case of the GoL, the Rhône waters deliver mainly illite and chlorite to
242 the Mediterranean Sea whereas rivers flowing from Massif Central, Corbières and Pyrénées
243 mainly carry illite and montmorillonite (Chamley, 1971). Thus, illite (K) is thought to be
244 abundant in fluvial waters ending in the GoL, and thus K relative abundances can be used as a
245 proxy for sediment continental provenance. Because illite might be depleted in K upon
246 pedogenetic processes, the K/Ti ratio can be considered as an indirect proxy for the intensity
247 of chemical weathering (Arnaud et al., 2012). The XRF raw data were smoothed using a 5-
248 point moving average to remove background noise.

249 In addition semi-quantitative bulk geochemical parameter such as total carbon (TC), organic
250 carbon (OC) and total nitrogen (TN) were determined from freeze-dried homogenized and
251 precisely weighed sub-samples of sediment using the Elementar Vario MAX CN automatic
252 elemental analyzer. Prior to the OC analyses, samples were acidified with 2M HCl overnight
253 at 50°C in order to remove carbonates (Cauwet et al., 1990). The precision of TC, OC and TN
254 measurements was 5 and 10%. The calcium carbonate content of the sediments was calculated
255 from TC-OC using the molecular mass ratio (CaCO_3 : C= 100:12). Results are expressed as
256 the weight percent of dry sediment (% d.w.). The atomic C:N ratio (C:N_a) was calculated and
257 used as a qualitative descriptor of organic matter (OM). Moloney and Field (1991a) proposed
258 $\text{C:N}_a = 6$ for OM of marine origin because of the high protein content of organisms such as
259 phytoplankton and zooplankton. Higher plant-derived OM of terrestrial origin have higher
260 C:N_a ratios (>20) than marine organisms because of a high percentage of non-protein
261 constituents (Meyers and Ishiwatari, 1993). In marine sediment, C:N_a ratios are usually higher
262 than phytoplankton. C:N_a ratios comprised between 6 and 10 are indicative of degraded
263 organic detritus resulting from the breakdown of the more labile nitrogenous compounds and



264 values of C:N_a ratio > 13 indicate a significant contribution of terrestrial organic matter (Goñi
265 et al., 2003).

266 The age model is based on 21 radiocarbon dates (Table 2) obtained by Accelerator Mass
267 Spectrometry (AMS) at the Laboratoire de Mesure du Carbone 14, Saclay (France). The two
268 uppermost dates were performed at Beta Analytic Radiocarbon Dating Laboratory and
269 indicate post-bomb values (AD 1950). The ¹⁴C dates were converted into 1σ calendar years
270 using Calib7.1 (Stuiver and Reimer, 1993) and the MARINE 13 calibration dataset including
271 the global marine reservoir age (400 years) (Charmasson et al., 1998). We used a local marine
272 reservoir age correction of ΔR = 23 ± 71 years (<http://calib.qub.ac.uk/marine/regioncalc.php>).
273 The age model was obtained by polynomial interpolation between ¹⁴C dates excluding the
274 minor reversal at 18.5 cm (350 ± 78 yrs) and the two post-bomb dates. Timing and
275 uncertainty of CR1 to CR6 is estimated using the Bayesian approach of OxCal 4.2 (Ramsey
276 and Lee, 2013) (Table 3). We used the same age model as in Jalali et al. (this volume). Age
277 inversions are not used in the estimation of the sedimentation rate (SR) (Table 2).

278

279 **4. Results**

280 **4.1. Age model, sedimentological core description**

281 Based on the 21 ¹⁴C dates, the average SR has been estimated to ~0.70 m/1,000 years. The
282 absolute chronology allows identifying three stratigraphic intervals corresponding to the
283 formal subdivision of the Holocene epoch proposed by (Walker et al., 2012). The well-known
284 cold events (Cold Relapses, CRs) are defined on the basis of this chronology (Figure 3, Table
285 1).

286 The core is predominantly composed of silt (60-70%) and clay. The clay content is highly
287 variable but no more than 50% between 10,000 and 4,000 a cal BP, and between 50 and 60%
288 in its upper 350 cm corresponding to the last 4,000 years (Figure 3). Small-size shell debris
289 are randomly mixed with the clayey silt but become more abundant between 400 and 500 cm
290 depth. Abundant and well-preserved *Turritella* sp shells certainly not reworked are found
291 between 680 and 640 cm. The sand fraction is generally very low (0.5-5%) except for the
292 lowermost 30 cm (50%, Figure 3). At visual inspection, the thin sandy base (between 703 and
293 690 cm) contains very abundant shell debris. Weak bioturbation is visible on the X-ray
294 images as well as the occurrence of sparse articulated shells.

295 Core KSGC31 was retrieved at the seaward edge of the Rhone mud belt. The seismic profile
296 at the position of the core displays the architecture of this mud belt that drapes Pliocene rocks



297 and continental deposits of the Last Glacial Maximum (Figure 2). The bottom of the core
298 corresponds to the *ravinement surface* (RS in Figure 2) that formed by wave erosion at the
299 time of marine flooding during the deglacial period. This heterolithic material includes fluvial
300 and coastal sands and gravels mixed with marine shells in a muddy matrix. At the position of
301 core KSGC31, it is postdated by the overlying muds immediately above (ca. 10,000 a cal BP).
302 The period of “turn around” between coastal retrogradation and coastal progradation is well
303 marked on the seismic profile by a downlap surface dated at ca. 7.5 ka cal BP at the position
304 of the core. It corresponds to the Maximum Flooding Surface in the sense of Posamentier and
305 Allen (1999). Two other distinct seismic surfaces (higher amplitude, slightly erosional) can
306 be recognized in the upper part of the wedge (Figure 2), they are dated at ca. 4.2 and 2.5 ka
307 cal BP from the core.

308 **4.2. Elemental and geochemical distribution**

309 Ca/Ti, K/Ti and Zr/Rb ratios were generated and cross-analyzed with grain-size (clay content
310 -D50 computed curve) and C:N_a to assess changes in geochemical composition.

311 **In the Early Holocene**, the Ca/Ti ratio is fairly constant and relatively high. The carbonate
312 content is high (>45% CaCO₃, Figure 4b), whereas C:N_a values are highly fluctuating
313 between values of 20 (~ 10 ka) and lower values of 13 towards the mid-Holocene (Figure 4a).
314 Zr/Rb ratios gradually decrease while K/Ti show a relatively stable behavior. Between 7,000
315 and 9,000 a cal BP, K/Ti and Zr/Rb indicate lower values, yet with a peak in the mid-interval,
316 around 8,200-8,300 a cal BP (Figure 4d,e). All over the period, clay content is comprised
317 approximately between 24 and 52% (Figure 5c), D50 is generally >10 μm and variable
318 (Figure 4f). A significant drop of Ca/Ti and D50 are observed in the 7,000-6,400 a cal BP
319 interval (Figure 4c, f). Similar trends are observed for the K/Ti and Zr/Rb, but the most abrupt
320 drop occurs between 6,500 and 6,400 a cal BP. No significant changes are detected in the
321 main lithology (mostly clayey, Figure 3). C:N_a ratios decrease (<13) due to a better
322 preservation of nitrogen in clay deposits.

323 **After 6.4 ka cal BP**, Ca/Ti a constant decreasing trend until 4,200 a cal BP. On the other
324 hand, C:N_a between 6,400 and 4,200 a cal BP reveals two prominent peaks (>15) culminating
325 at 5,700 and 4,800 a cal BP (Figure 4a) that roughly correspond to low K/Ti and Zr/Rb values
326 (Figure 4d, e), higher clay (Figure 5c) and lower carbonate sediment contents (Figure 4b).
327 The most pronounced changes in the elemental ratio are observed after 4,200 a cal BP
328 (Figures 4 and 5). Millennial-scale oscillations are discernible in the Ca/Ti record (Figure 4c)
329 and coherent with changes in K/Ti and Zr/Rb ratios (Figure 4d, e) and, to some extent, with



330 the D50 values (Figure 4f). Six main episodes of high terrigenous inputs (lowest Ca/Ti) are
331 clearly expressed in the XRF data at $\sim 3,500 \pm 170$, $\sim 2,840 \pm 172$, $\sim 2,200 \pm 145$, $\sim 1,500 \pm$
332 124 , $\sim 1,010 \pm 75$ and $\sim 720 \pm 72$ a cal BP (Figure 4, Table 4). Considering the age
333 uncertainty, only some of those events might coincide with CRs (CR6, CR5, CR4, Figure 4).
334 The peaks in the clay content correspond to low Ca/Ti ratios of variable amplitude. The clay
335 content of the 2,840 and 2,200 a cal BP events are among the highest ($\sim 35\%$, Figure 5e).
336 From 4,200 a cal BP to present, the C:N_a values decrease gradually. Between $\sim 4,200$ and
337 3,200 a cal BP, some values exceed 13. Thereafter, the C:N_a values range between 9 and 10
338 (Figure 4a). The Late Holocene is also characterized by decreasing carbonate content with a
339 drastic drop around 2,000 a cal BP (Figure 4b). The SR is also higher than during the Mid-
340 Holocene lying between 0.5 and 1 mm/year.

341

342 **5. Discussion**

343 *Early Holocene (11.7-8.2 ka cal BP)*

344 Based on seismic evidences, the KSGC31 basal deposits correspond to the early setting of the
345 mud belt unconformably lying on older fluvial sediments (Figure 2). The mud belt initiation
346 phase is marked by coarse (silty-sand) grained sediments (coastal and deltaic) with abundant
347 shell debris transported when the relative sea-level was -30/40 m lower than today. This
348 interval is marked by highest SR values and high terrestrial supply as also indicated by the
349 high C:N_a ratio (>13) (Figure 4a) (Buscail and Germain, 1997; Buscail et al., 1990; Gordon
350 and Goñi, 2003; Kim et al., 2006). Of note, the C:N_a ratios ~ 20 indicative of even larger
351 enrichment in organic material originating from soils or plant debris in the coarse deposit at
352 the very bottom of the core (700 cm) (Hedges and Oades, 1997; Meyers, 1993 #2518; Meyers
353 and Ishiwatari, 1993). A layer of high *Turritella* abundances is identified in the fine-grained
354 sediments just above the sandy interval (680-640 cm, i.e. 8,500 -8,000 a cal BP) (Figure 3).
355 Then *Turritella* shells disappear gradually towards the top of the core, suggesting an upward
356 deepening environment. The high *Turritella* level could indicate a change in Northern
357 Hemisphere climate and can be hypothetically related to the “*Turritella* Layer” described by
358 Naughton et al. (2007) on the NW Atlantic shelf, therefore suggesting a regional change
359 between 8,700 and 8,400 a cal BP, possibly in relation with the southward migration of the
360 Boreal biogeographical zone. The Maximum Flooding Surface (MSF) is dated around 7,500 a
361 cal BP (Figure 2). This age may vary at different locations because it depends upon the ratio
362 between sediment delivery and accommodation space, but it matches well the age of delta
363 initiations observed worldwide by Stanley and Warne (1994).



364 The increase of K/Ti between 9,000 and 7,000 a cal BP might reflect the gradual decrease of
365 the contribution of weathered material from the river catchment areas, which can thus be
366 interpreted as a signal of weaker pedogenetic processes and lower soil erosion due to dry
367 climate in European Alps (Figure 4d) (Arnaud et al., 2012).

368 The period between ~ 12,000 and 7,000 a cal BP is marked by a continuous retreat of Arctic
369 continental ice-sheets until the complete disappearance of the Fennoscandian and Laurentide
370 ice cap (Tornqvist and Hijma, 2012; Ullman et al., 2015). Ice sheet melting is seen in the
371 general sea-level rise and also manifested by short-lived water releases into the ocean when
372 sufficient enough to perturb the North Atlantic Ocean circulation and climate over Europe (for
373 example the 8,200 cal BP event, here CR0). It is worthwhile to note that around CR0, the
374 K/Ti ratio shows a peak within an interval of low values between approximately 7,900 and
375 8,300 a cal BP. This peak would identify an increase of continental supply and low chemical
376 weathering corresponding to cold (weak soil formation) and wet (high physical erosion)
377 conditions over mid-latitude Europe in response to the 8,200 a cal BP cooling (Arnaud et al.,
378 2012; Magny et al., 2003) also attested by higher lake levels in Western Europe (Figure 5d, f)
379 concurrent with CR0 (Magny et al., 2013). Note that no clear temperature drop in the
380 alkenone-derived SST record generated in the core has been detected (Jalali et al., this
381 volume).

382

383 *Mid-Holocene (8.2-4.2 ka cal BP)*

384 Values of Ca/Ti and C:N_a ratios indicate a progressive increase of terrestrial inputs (Figure
385 4ac) during the Mid-Holocene, despite increasing distance of KSGC31 site from river outlets
386 due to sea-level rise and the progressive shift of the Rhone delta to the East (Fanget et al.,
387 2014).

388 The Ca/Ti ratio values drop drastically between 7,000 and 6,400 a cal BP. In Eastern
389 Mediterranean enhanced sediment delivery is documented around 7,000 a cal BP (Castañeda
390 et al., 2016; Skonieczny et al., 2015) during the Saharan Humid Period (SHP). In Western
391 Mediterranean, torrential discharges are observed in most rivers of Southern France and
392 thought to be responsible for a regional episode of river incision between 7,200 and 6,800
393 a cal BP (Benito et al., 2015). These events coincides with the deposition of large amount of
394 fine-grained sediments at the site of KSGC31 (Figure 4). We thus hypothesize high fluvial
395 activity between 7,000 and 6,400 a cal BP, coinciding with fine-grained deposits, the coarser
396 fraction being trapped in the deltaic system (Fanget et al., 2014). Possible connections
397 between runoff from the South Mediterranean as a consequence of a strengthened North



398 African monsoon and increased precipitations over the Mediterranean basin itself have been
399 recently investigated (Bosmans et al., 2015; Kutzbach et al., 2013).

400 Our observations raise the question if an increase in the discharge of NW Mediterranean
401 rivers might be synchronous with the SHP. Some climate archives like speleothems and lake
402 records show evidence for a substantial increase in precipitation both in the Western and
403 Eastern Mediterranean (Zanchetta et al., 2007; Zhornyak et al., 2011). However, in the case of
404 Rhone River, we cannot rule out the possibility that alpine glacier meltwater could have at
405 least in part contributed to increase the Rhone River discharge.

406 The Mid-Holocene is described as a period of relatively mild and high atmospheric moisture
407 balance (Cheddadi et al., 1998) that favored the maximum expansion of the mesophytic forest
408 leading to a maximum land cover over Europe. Nonetheless, two main short-lived climate
409 anomalies are reported at 6,600–5,700 a cal BP (CR1, Tables 2 and 3) and 5,300–5,000 a cal
410 BP (CR2, Tables 2 and 3) over the North Atlantic (Wanner et al., 2011) and in Europe
411 (Magny and Haas, 2004; Roberts et al., 2011a; Roberts et al., 2011b), at the time of global
412 cooling. CR1 is associated with drying climate in eastern Europe and Asia and has been
413 related to the weakening of the Asian monsoon and the decrease of summer insolation (Gasse
414 et al., 1991), while CR2 coincides with weaker solar activity as indicated by maximum
415 atmospheric ^{14}C around 5,600–5,200 a cal BP (Stuiver et al., 2006), lower tree lines (Magny
416 and Haas, 2004) and colder sea-surface temperatures (Jalali et al., this volume).

417 According to our data, during CR1 and CR2, there was no significant change in terrigenous
418 inputs (Ca/Ti ratio, Figure 4c), mean SR was generally low (<1 mm/yr on average, Table 2)
419 and chemical weathering was weak as suggested by high K/Ti values (Figure 4d). The C:N_a
420 ratios indicate better preservation of nitrogen organic compounds preferentially adsorbed in
421 the clay fraction (Figure 4a). The reduction of the vegetation cover in the river catchment,
422 combined with lower (1–1.5°C) temperatures in the European Alps (Haas et al., 1998), may
423 explain the low chemical degradation state of the illite minerals. A drop in sea surface
424 temperature is also recorded by alkenones in the core (Jalali et al., this volume), confirming
425 the global climate impact of the cold relapses in the Mediterranean area (Figure 4i).

426

427 *Late Holocene (4.2–0 ka cal BP)*

428 Multi-decadal to century-scale wet episodes are evidenced from ~ 4,200 a cal BP, that marks
429 the Mid-Late Holocene transition (Figure 3). In the KSGC31 core, wetter intervals are
430 expressed by highly fluctuating Ca/Ti, Zr/Rb and K/Ti ratios, C:N_a and grain size values.



431 From present to 3.5 ka cal BP, the C:N_a ratio shows an increase from 9 to 11 (Figure 4)
432 testifying active diagenetic processes, due to preferential degradation of nitrogen relative to
433 carbon during burial. Some values > 13 are still observed between 4,200 and 3,500 a cal BP,
434 indicating enhanced terrestrial inputs. Episodes of enhanced terrigenous inputs are detected by
435 low Ca/Ti ratios that also coincide with low Zr/Rb and low D50 values, indicating general
436 smaller-size terrigenous grains as also suggested by high clay content (Figure 5c). Thus,
437 intensified hydrological activity associated with high terrestrial inputs would have prevailed
438 during the Late Holocene, as also suggested by higher SR (Table 2). The enhanced terrestrial
439 inputs are inferred from XRF ratios discussed here, but also by the biomarker data. Indeed,
440 Jalali et al. (this volume) also highlighted enhanced flood activity during the Late Holocene
441 based on TERR-alkane concentrations, which are among the highest of the entire Holocene
442 record.

443 A similar signature of continental runoff in marine sediments (low Ca/Ti ratio) during the past
444 ~ 6,500 years has been reported in the central Mediterranean and related to climatically driven
445 wet periods (Moloney and Field, 1991b). Indeed, some of these events (~2840 a, ~ 1500 and
446 ~720 a cal BP) encompass cold events in the North Atlantic (LIA-CR6; Dark Age-CR5; CR4,
447 Figure 4) and coincide with periods of increasing flood frequency in the Northern Alps as
448 reconstructed by Wirth et al. (2013) (Figure 5d). However, other humid episodes occur during
449 warmer periods such as the MCA at ~ 3,500; ~ 2,200 and ~1,000 a cal BP (Figure 4)
450 suggesting different causes for enhanced precipitations.

451 The North Atlantic Oscillation (NAO) exerts a strong influence on the precipitation pattern in
452 Europe and the NW Mediterranean region. Today, precipitation in the western Mediterranean
453 region and southern France is lower during positive NAO. Rainfall increases under negative
454 NAO due to the southern shift of the Atlantic storm tracks leading to enhanced cyclogenesis
455 in the Mediterranean Sea (Trigo et al., 2000). The position of the ITCZ is also important in
456 the precipitation pattern of the Mediterranean region and its southernmost position is the
457 probable cause for extremely dry conditions between 2,500 and 2,000 a cal BP
458 (Schimmelfennig et al., 2012). The reconstructed NAO index (Olsen et al., 2012) indicates a
459 predominance of positive state between 5,000-4,500 and 2,000-550 a cal BP, in agreement
460 with a) an increased frequency of floods in Northern Alps (Wirth et al., 2013), b) higher lake
461 levels at Accessa (Central Italy), Ledro (Northern Italy) and in Central-Western Europe
462 (Magny et al., 2013), all together suggesting more humid conditions in west-central Europe
463 (Figure 5). However, between 2,500 and 2,000 a cal BP, very negative NAO and



464 southernmost position of the ITCZ (Haug et al., 2001) would have led to several centuries of
465 extreme dryness.

466 Late Holocene human settlements along the Rhone valley and South France may have had an
467 impact on the origin and amounts of eroded sediments in the river catchment areas. When
468 examining the chemical signature of KSGC-31 sediments, low K/Ti ratios co-eval with wet
469 events (Figure 4d) reflecting soil weathering due to terrain degradation, that could be
470 interpreted as the result of widespread deforestation for agropastoral activities in this area
471 since the end of the Neolithic. The most extensive erosion episodes in the Rhone valley
472 correspond to 1) the end of Neolithic (~ 4,000 BC; 6,000 a cal BP) after the first phase of
473 human expansion linked to the development of the agriculture 2) the end of the Bronze Age
474 (~ 2,000 BC; 4,000 a cal BP) and 3) the Roman Period when a rapid transformation of
475 landscape is operated by deforestation and their replacement by intensively cultivated
476 agricultural land (van der Leeuw, 2005).

477 Disentangling human impact from climate control on environmental changes in the Late
478 Holocene is not an easy task, and requires the study of other river catchment basins to confirm
479 the regional character of these observations. However, assuming that climate variability is the
480 major factor influencing soil pedogenesis, we can hypothesize that the elemental composition
481 of marine sediments reflects erosion and transport because of a good correspondence with
482 temperature variability in the Mediterranean Sea (Jalali et al., this volume), and because, on a
483 regional scale, both marine and continental climate proxies indicate co-eval signals. Despite
484 the fact that the characteristics in amplitude and duration of these climate intervals slightly
485 differ geographically, there seems to be a general agreement on their origin and the role of
486 solar forcing and large-scale atmospheric circulation. However, amplification of soil
487 degradation following human occupation waves should be further explored through accurate
488 correlation between archeological data and paleoenvironmental proxies in order to better
489 evaluate the importance of land use on sedimentary signals.

490

491 **6. Conclusions**

492 This work represents the first attempt to detect and decipher the linkages between rapid
493 climate changes and continental paleo-hydrology in the NW Mediterranean shallow marine
494 setting during the Holocene.

495 Based on the combination of sedimentological and geochemical proxies we could
496 demonstrate that between 11 and 4 ka cal BP, terrigenous input broadly increased and reached



497 a maximum around 7,000 a cal BP probably as a result of a more humid phase. From ca.
498 4,000 a cal BP to present, the sediment flux proxies indicate enhanced variability in the
499 amount of land-derived material delivered to the Mediterranean by the Rhone River input. We
500 suggest that this late Holocene variability is due to changes in large-scale atmospheric
501 circulation and rainfall patterns in Western Europe including the variability of continental
502 glaciers. Anthropogenic impact such as deforestation resulting in higher sediment flux into
503 the Gulf of Lions are also likely and should be better taken into account in the future.

504 **Acknowledgements**

505 We would like to thank MISTRALS/PALEOMEX for financial support and the crew operating the
506 GMO2 Carnac (R/V “Le Suroît”) and GolHo(R/V “Néréis”) cruises. Nabil Sultan and the crew and
507 science parties aboard R/V Suroit (IFREMER) retrieved core KSGC31 during the GMO2-
508 Carnac cruise. The Captain and crew of R/V Néréis (Observatoire Océanologique de
509 Banyuls), as well as Olivier Raynal and Raphael Certain (CEFREM) are thanked for their
510 assistance during the MADHO 1 cruise. ARTEMIS (Saclay, France) program is
511 acknowledged for performing the ¹⁴C measurements.

512



513

514

References

- 515 Aloisi, J. C., Auffret, G. A., Auffret, J. P., Barusseau, J. P., Hommeril, P., Larssonneur, C., and
516 Monaco, A.: Essai de modelisation de la sedimentation actuelle sur les plateaux continentaux
517 francais, Bulletin de la Societe Geologique de France, Series 7 Vol. XIX, 183-195, 1977.
- 518 Anchukaitis, K. and Tierney, J.: Identifying coherent spatiotemporal modes in time-uncertain proxy
519 paleoclimate records, *Climate Dynamics*, 41, 1291-1306, 2013.
- 520 Arnaud-Fassetta, G.: Dynamiques fluviales holocenes dans le delta du Rhône, 1998.PhD, UFR des
521 Sciences Géographiques, Université de Provence, Aix en Provence, 329 pp., 1998.
- 522 Arnaud-Fassetta, G.: The Upper Rhône Delta Sedimentary Record in the Arles-Piton Core: Analysis
523 of Delta-Plain Subenvironments, Avulsion Frequency, Aggradation Rate and Origin of Sediment
524 Yield, *Geografiska Annaler: Series A, Physical Geography*, 86, 367-383, 2004.
- 525 Arnaud-Fassetta, G., Carcaud, N., Castanet, C., and Salvador, P. G.: Fluvatile palaeoenvironments in
526 archaeological context: Geographical position, methodological approach and global change –
527 Hydrological risk issues, *Quaternary International*, 216, 93-117, 2010.
- 528 Arnaud-Fassetta, G., De Beaulieu, J.-L., Suc, J.-P., Provansal, M., Williamson, D., Leveau, P., Aloisi,
529 J.-C., Gadel, F., Giresse, P., Oberlin, C., and Duzer, D.: Evidence for an early land use in the
530 Rhône delta (Mediterranean France) as recorded by late Holocene fluvial paleoenvironments
531 (1640–100 BC), *Geodinamica Acta*, 13, 377-389, 2000.
- 532 Arnaud, F., Révillon, S., Debret, M., Revel, M., Chapron, E., Jacob, J., Giguet-Covex, C., Poulenard,
533 J., and Magny, M.: Lake Bourget regional erosion patterns reconstruction reveals Holocene NW
534 European Alps soil evolution and paleohydrology, *Quaternary Science Reviews*, 51, 81-92, 2012.
- 535 Barber, D. C., Dyke, A., Hillaire-Marcel, C., Jennings, A. E., Andrews, J. T., Kerwin, M. W.,
536 Bilodeau, G., McNeely, R., Southon, J., Morehead, M. D., and Gagnon, J. M.: Forcing of the cold
537 event of 8,200 years ago by catastrophic drainage of Laurentide lakes, *Nature*, 400, 344-348, 1999.
- 538 Bassetti, M. A., Jouet, G., Dufois, F., Berne, S., Rabineau, M., and Taviani, M.: Sand bodies at the
539 shelf edge in the Gulf of Lions (Western Mediterranean): Deglacial history and modern processes,
540 *Marine Geology*, 234, 93-109, 2006.
- 541 Benito, G., Macklin, M. G., Zielhofer, C., Jones, A. F., and Machado, M. J.: Holocene flooding and
542 climate change in the Mediterranean, *CATENA*, 130, 13-33, 2015.
- 543 Benito, G., Sopena, A., Sánchez-Moya, Y., Machado, M. a. J., and Pérez-González, A.: Palaeoflood
544 record of the Tagus River (Central Spain) during the Late Pleistocene and Holocene, *Quaternary
545 Science Reviews*, 22, 1737-1756, 2003.
- 546 Berné, S. and Gorini, C.: The Gulf of Lions: An overview of recent studies within the French 'Margins'
547 programme, *Marine and Petroleum Geology*, 22, 691-693, 2005.
- 548 Berné, S., Jouet, G., Bassetti, M. A., Dennielou, B., and Taviani, M.: Late Glacial to Preboreal sea-
549 level rise recorded by the Rhone deltaic system (NW Mediterranean), *Marine Geology*, 245, 65-88,
550 2007.
- 551 Berné, S., Rabineau, M., Flores, J. A., and Sierro, F. J.: The impact of Quaternary Global Changes on
552 Strata Formation. Exploration of the shelf edge in the Northwest Mediterranean Sea,
553 *Oceanography*, 17, 92-103, 2004.
- 554 Bonneau, L., Jorry, S. J., Toucanne, S., Jacinto, R. S., and Emmanuel, L.: Millennial-Scale Response
555 of a Western Mediterranean River to Late Quaternary Climate Changes: A View from the Deep
556 Sea, *The Journal of Geology*, 122, 687-703, 2014.
- 557 Bosmans, J. H. C., Drijfhout, S. S., Tuenter, E., Hilgen, F. J., Lourens, L. J., and Rohling, E. J.:
558 Precession and obliquity forcing of the freshwater budget over the Mediterranean, *Quaternary
559 Science Reviews*, 123, 16-30, 2015.
- 560 Buscaïl, R. and Germain, C.: Present-day organic matter sedimentation on the NW Mediterranean
561 margin: Importance of off-shelf export, *Limnology and Oceanography*, 42, 217-229, 1997.
- 562 Buscaïl, R., Pocklington, R., Dumas, R., and Guidi, L.: Fluxes and budget of organic matter in the
563 benthic boundary layer over the northwestern Mediterranean margin, *Continental Shelf research*,
564 10, 1089-1122, 1990.



- 565 Calmet, D. and Fernandez, J.-M.: Caesium distribution in northwest Mediterranean seawater,
 566 suspended particles and sediment, *Continental Shelf research*, 10, 895-913, 1990.
- 567 Castañeda, I. S., Schouten, S., Pätzold, J., Lucassen, F., Kasemann, S., Kuhlmann, H., and Schefuß,
 568 E.: Hydroclimate variability in the Nile River Basin during the past 28,000 years, *Earth and
 569 Planetary Science Letters*, 438, 47-56, 2016.
- 570 Cattaneo, A., Correggiari, A., Langone, L., and Trincardi, F.: The late-Holocene Gargano subaqueous
 571 delta, Adriatic shelf: Sediment pathways and supply fluctuations, *Marine Geology*, 193, 61-91,
 572 2003.
- 573 Cauwet, G., Gadel, F., de Souza Sierra, M. M., Donard, O., and Ewald, M.: Contribution of the
 574 Rhône River to organic carbon inputs to the northwestern Mediterranean Sea, *Continental Shelf
 575 Research*, 10, 1025-1037, 1990.
- 576 Chambers, F. M., Mauquoy, D., Brain, S. A., Blaauw, M., and Daniell, J. R. G.: Globally synchronous
 577 climate change 2800 years ago: Proxy data from peat in South America, *Earth and Planetary
 578 Science Letters*, 253, 439-444, 2007.
- 579 Chamley, H.: Recherches sur la sédimentation argileuse en Méditerranée, PhD, Université Aix-en-
 580 Marseille, 209 pp., 1971.
- 581 Charmasson, S., Radakovitch, O., Arnaud, M., Bouisset, P., and Pruchon, A.-S.: Long-core profiles
 582 of ^{137}Cs , ^{134}Cs , ^{60}Co and ^{210}Pb in sediment near the Rhône River (Northwestern Mediterranean
 583 Sea), *Estuaries*, 21, 367-378, 1998.
- 584 Cheddadi, R., Lamb, H. F., Guiot, J., and van der Kaars, S.: Holocene climatic change in Morocco: a
 585 quantitative reconstruction from pollen data, *Climate Dynamics*, 14, 883-890, 1998.
- 586 Cronin, T. and Raymo, M.: Orbital forcing of deep-sea benthic species diversity, *Nature*, 385, 624-
 587 627, 1997.
- 588 Cronin, T. M., Boomer, I., Dwyer, G. S., and Rodriguez-Lazaro, J.: Ostracoda and Paleoceanography.
 589 In: *The Ostracoda: Applications in Quaternary Research*, American Geophysical Union, 2002.
- 590 Cronin, T. M., Polyak, L., Reed, D., Kandiano, E. S., Marzen, R. E., and Council, E. A.: A 600-ka
 591 Arctic sea-ice record from Mendeleev Ridge based on ostracodes, *Quaternary Science Reviews*, 79,
 592 157-167, 2013.
- 593 Do Carmo, D. A. and Sanguinetti, Y. T.: Taxonomy and palaeoceanographical significance of the
 594 genus *Krithe* (Ostracoda) in the Brazilian margin, *Journal of Micropalaeontology*, 18, 111-123,
 595 1999.
- 596 Durrieu De Madron, X., Abassi, A., Heussner, S., Monaco, A., Aloisi, J. C., Radakovitch, O., Giresse,
 597 P., Buscail, R., and Kerherve, P.: Particulate matter and organic carbon budgets for the Gulf of
 598 Lions (NW Mediterranean), *Oceanologica Acta*, 23, 717-730, 2000.
- 599 Dypvik, H. and Harris, N. B.: Geochemical facies analysis of fine-grained siliciclastics using Th/U,
 600 Zr/Rb and (Zr+Rb)/Sr ratios, *Chemical Geology*, 181, 131-146, 2001.
- 601 Estournel, C., Durrieu de Madron, X., Marsaleix, P., Auclair, F., Julliand, C., and Vehil, R.:
 602 Observation and modeling of the winter coastal oceanic circulation in the Gulf of Lion under wind
 603 conditions influenced by the continental orography (FETCH experiment), *J. Geophys. Res.*, 108,
 604 8059, 2003.
- 605 Evans, M. N., Tolwinski-Ward, S. E., Thompson, D. M., and Anchukaitis, K. J.: Applications of proxy
 606 system modeling in high resolution paleoclimatology, *Quaternary Science Reviews*, 76, 16-28,
 607 2013.
- 608 Eyrolle, F., Radakovitch, O., Raimbault, P., Charmasson, S., Ferrand, E., Antonelli, C., Jacquet, S.,
 609 Aubert, D., Raccasi, G., and Gurriaran, R.: Hydrological events on suspended sediment and
 610 associated radionuclide deliveries from the Rhône River towards the Mediterranean Sea, *Journal of
 611 Soils and Sediments*, DOI, 10, 2012.
- 612 Fanget, A.-S., Berné, S., Jouet, G., Bassetti, M.-A., Dennielou, B., Maillet, G. M., and Tondut, M.:
 613 Impact of relative sea level and rapid climate changes on the architecture and lithofacies of the
 614 Holocene Rhone subaqueous delta (Western Mediterranean Sea), *Sedimentary Geology*, 305, 35-
 615 53, 2014.
- 616 Fanget, A. S., Bassetti, M. A., Arnaud, M., Chiffolleau, J. F., Cossa, D., Goineau, A., Fontanier, C.,
 617 Buscail, R., Jouet, G., Maillet, G. M., Negri, A., Dennielou, B., and Berné, S.: Historical evolution
 618 and extreme climate events during the last 4000 years on the Rhone prodelta (NW
 619 Mediterranean), *Marine Geology*, 346, 375-391, 2013.



- 620 Faust, D., Zielhofer, C., Baena Escudero, R., and Diaz del Olmo, F.: High-resolution fluvial record of
 621 late Holocene geomorphic change in northern Tunisia: climatic or human impact?, *Quaternary*
 622 *Science Reviews*, 23, 1757-1775, 2004.
- 623 Fletcher, W. J. and Sánchez Goñi, M. F.: Orbital- and sub-orbital-scale climate impacts on vegetation
 624 of the western Mediterranean basin over the last 48,000 yr, *Quaternary Research*, 70, 451-464,
 625 2008.
- 626 Fontanier, C., Jorissen, F. J., Chaillou, G., Anschutz, P., Grémare, A., and Griveaud, C.: Live
 627 foraminiferal faunas from a 2800m deep lower canyon station from the Bay of Biscay:
 628 Faunal response to focusing of refractory organic matter, *Deep Sea Research Part I: Oceanographic*
 629 *Research Papers*, 52, 1189-1227, 2005.
- 630 Fontanier, C., Mackensen, A., Jorissen, F. J., Anschutz, P., Licari, L., and Griveaud, C.: Stable oxygen
 631 and carbon isotopes of live benthic foraminifera from the Bay of Biscay: Microhabitat impact and
 632 seasonal variability, *Marine Micropaleontology*, 58, 159-183, 2006.
- 633 Frezza, V. and Carboni, M. G.: Distribution of recent foraminiferal assemblages near the Ombrone
 634 River mouth (Northern Tyrrhenian Sea, Italy), *Revue de Micropaléontologie*, 52, 43-66, 2009.
- 635 Gasse, F., Arnold, M., Fontes, J. C., Fort, M., Gibert, E., Huc, A., Bingyan, L., Yuanfang, L., Qing, L.,
 636 Melieres, F., Campo, E. V., Fubao, W., and Qingsong, Z.: A 13,000-year climate record from
 637 western Tibet, *Nature*, 353, 742-745, 1991.
- 638 Gensous, B. and Tesson, M.: L'analyse des dépôts postglaciaires et son application à l'étud des
 639 séquences de dépôt du Quaternaire terminal sur la plate-forme au large du Rhône (golfe du Lion),
 640 *Bulletin de la Société Géologique de France*, 174, 401-419, 2003.
- 641 Goñi, M. A., Teixeira, M. J., and Perkey, D. W.: Sources and distribution of organic matter in a river-
 642 dominated estuary (Winyah Bay, SC, USA), *Estuarine, Coastal and Shelf Science*, 57, 1023-1048,
 643 2003.
- 644 Gordon, E. S. and Goñi, M. A.: Sources and distribution of terrigenous organic matter delivered by the
 645 Atchafalaya River to sediments in the northern Gulf of Mexico, *Geochimica et Cosmochimica*
 646 *Acta*, 67, 2359-2375, 2003.
- 647 Haas, J. N., Richoz, I., Tinner, W., and Wick, L.: Synchronous Holocene climatic oscillations recorded
 648 on the Swiss Plateau and at timberline in the Alps, *The Holocene*, 8, 301-309, 1998.
- 649 Haug, G. H., Hughen, K. A., Sigman, D. M., Peterson, L. C., and Röhl, U.: Southward Migration of
 650 the Intertropical Convergence Zone Through the Holocene, *Science*, 293, 1304-1308, 2001.
- 651 Hedges, J. I. and Oades, J. M.: Comparative organic geochemistries of soils and marine sediments,
 652 *Organic Geochemistry*, 27, 319-361, 1997.
- 653 Hill, P. S., Fox, J. S., J.S., C., Kurran, K. J., Friedrichs, C. T., Geyer, W. R., Milligan, T. G., Ogston,
 654 A. P., Puig, P., M.E., S., P.A., T., and Wheatcroft, W. G.: Sediment delivery to the seabed on
 655 continental margins, *IAS Special Publication* 37, 49-99, 2007.
- 656 Ishihama, S., Oi, T., Hasegawa, S., and Matsumoto, R.: Paleoceanographic changes of surface and
 657 deep water based on oxygen and carbon isotope records during the last 130 kyr identified in
 658 MD179 cores, off Joetsu, Japan Sea, *Journal of Asian Earth Sciences*, 90, 254-265, 2014.
- 659 Ishihama, S., Oi, T., Hasegawa, S., and Matsumoto, R.: Paleoceanographic changes of surface and
 660 deep water based on oxygen and carbon isotope records during the last 130 kyr identified in
 661 MD179 cores, off Joetsu, Japan Sea, *Journal of Asian Earth Sciences*, doi:
 662 <http://dx.doi.org/10.1016/j.jseaes.2013.12.020>.
- 663 Josey, S. A., Somot, S., and Tsimplis, M.: Impacts of atmospheric modes of variability on
 664 Mediterranean Sea surface heat exchange, *Journal of Geophysical Research: Oceans*, 116, n/a-n/a,
 665 2011.
- 666 Jouet, G.: Enregistremets stratigraphiques des cycles climatiques et glacio-eustatiques du Quaternaire
 667 terminal. Modélisation de la marge continentale du Golfe du Lion, 2007. Université de Bretagne
 668 Occidentale, Brest, 443 pp., 2007.
- 669 Kim, J.-H., Schouten, S., Buscail, R., Ludwig, W., Bonnin, J., Sinninghe Damsté, J. S., and Bourrin,
 670 F.: Origin and distribution of terrestrial organic matter in the NW Mediterranean (Gulf of Lions):
 671 Exploring the newly developed BIT index, *Geochemistry, Geophysics, Geosystems*, 7, n/a-n/a,
 672 2006.
- 673 Konert, M. and Vandenberghe, J. E. F.: Comparison of laser grain size analysis with pipette and sieve
 674 analysis: a solution for the underestimation of the clay fraction, *Sedimentology*, 44, 523-535, 1997.



- 675 Kutzbach, J. E., Chen, G., Cheng, H., Edwards, R. L., and Liu, Z.: Potential role of winter rainfall in
676 explaining increased moisture in the Mediterranean and Middle East during periods of maximum
677 orbitally-forced insolation seasonality, *Climate Dynamics*, 42, 1079-1095, 2013.
- 678 L'Homer, A., Bazile, F., Thommeret, J., and Thommeret, Y.: Principales étapes de l'édification du
679 delta du Rhône de 7000 B.P. à nos jours ; variations du niveau marin, *Oceanis*, 7, 389-408, 1981.
- 680 Lombo Tombo, S., Dennielou, B., Berné, S., Bassetti, M. A., Toucanne, S., Jorry, S. J., Jouet, G., and
681 Fontanier, C.: Sea-level control on turbidite activity in the Rhone canyon and the upper fan during
682 the Last Glacial Maximum and Early deglacial, *Sedimentary Geology*, 323, 148-166, 2015.
- 683 Magny, M., Bégeot, C., Guiot, J., and Peyron, O.: Contrasting patterns of hydrological changes in
684 Europe in response to Holocene climate cooling phases, *Quaternary Science Reviews*, 22, 1589-
685 1596, 2003.
- 686 Magny, M., Combourieu-Nebout, N., de Beaulieu, J. L., Bout-Roumazielles, V., Colombaroli, D.,
687 Desprat, S., Francke, A., Joannin, S., Ortu, E., Peyron, O., Revel, M., Sadori, L., Siani, G., Sicre,
688 M. A., Samartin, S., Simonneau, A., Tinner, W., Vannièrè, B., Wagner, B., Zanchetta, G.,
689 Anselmetti, F., Brugiapaglia, E., Chapron, E., Debret, M., Desmet, M., Didier, J., Essallami, L.,
690 Galop, D., Gilli, A., Haas, J. N., Kallel, N., Millet, L., Stock, A., Turon, J. L., and Wirth, S.: North-
691 South palaeohydrological contrasts in the central Mediterranean during the Holocene: tentative
692 synthesis and working hypotheses, *Clim. Past*, 9, 2043-2071, 2013.
- 693 Magny, M. and Haas, J. N.: A major widespread climatic change around 5300 cal. yr BP at the time of
694 the Alpine Iceman, *Journal of Quaternary Science*, 19, 423-430, 2004.
- 695 Meyers, P. A. and Ishiwatari, R.: Lacustrine organic geochemistry—an overview of indicators of
696 organic matter sources and diagenesis in lake sediments, *Organic Geochemistry*, 20, 867-900,
697 1993.
- 698 Millot, C.: The Gulf of Lions' hydrodynamics, *Continental Shelf Research*, 10, 885-894, 1990.
- 699 Moloney, C. and Field, J.: Modelling Carbon and Nitrogen Flows in a Microbial Plankton
700 Community. In: *Protozoa and Their Role in Marine Processes*, Reid, P. C., Turley, C. M., and
701 Burkill, P. H. (Eds.), NATO ASI Series, Springer Berlin Heidelberg, 1991a.
- 702 Moloney, C. L. and Field, J. G.: The size-based dynamics of plankton food webs. I. A simulation
703 model of carbon and nitrogen flows, *Journal of Plankton Research*, 13, 1003-1038, 1991b.
- 704 Monaco, A., Courp, T., Heussner, S., Carbonne, J., Fowler, S. W., and Deniaux, B.: Seasonality and
705 composition of particulate fluxes during ECOMARGE--I, western Gulf of Lions, *Continental Shelf
706 Research*, 10, 959-987, 1990.
- 707 Müller, P. J. and Suess, E.: Productivity, sedimentation rate, and sedimentary organic matter in the
708 oceans—I. Organic carbon preservation, *Deep Sea Research Part A. Oceanographic Research
709 Papers*, 26, 1347-1362, 1979.
- 710 Naudin, J. J., Cauwet, G., Chrétiennot-Dinet, M. J., Deniaux, B., Devenon, J. L., and Pauc, H.: River
711 Discharge and Wind Influence Upon Particulate Transfer at the Land–Ocean Interaction: Case
712 Study of the Rhone River Plume, *Estuarine, Coastal and Shelf Science*, 45, 303-316, 1997.
- 713 Naughton, F., Bourillet, J.-F., Sánchez Goñi, M. F., Turon, J.-L., and Jouanneau, J.-M.: Long-term and
714 millennial-scale climate variability in northwestern France during the last 8850 years, *The
715 Holocene*, 17, 939-953, 2007.
- 716 Olsen, J., Anderson, N. J., and Knudsen, M. F.: Variability of the North Atlantic Oscillation over the
717 past 5,200 years, *Nature Geosci*, 5, 808-812, 2012.
- 718 PAGES 2k Consortium: Continental-scale temperature variability during the past two millennia,
719 *Nature Geosci*, 6, 339-346, 2013.
- 720 Perez-Sanz, A., Li, G., González-Sampériz, P., and Harrison, S. P.: Evaluation of modern and mid-
721 Holocene seasonal precipitation of the Mediterranean and northern Africa in the CMIP5
722 simulations, *Clim. Past*, 10, 551-568, 2014.
- 723 Petrenko, A. A.: Variability of circulation features in the Gulf of Lion NW Mediterranean Sea.
724 Importance of inertial currents, *Oceanologica Acta*, 26, 323-338, 2003.
- 725 Pont, D., Simonnet, J. P., and Walter, A. V.: Medium-term Changes in Suspended Sediment Delivery
726 to the Ocean: Consequences of Catchment Heterogeneity and River Management (Rhône River,
727 France), *Estuarine, Coastal and Shelf Science*, 54, 1-18, 2002.
- 728 Posamentier, H. W. and Allen, G. P.: Siliciclastic sequence stratigraphy: concepts and applications,
729 *Society for Sedimentary Geology, Tulsa*, 1999.



- 730 Puig, P., Ogston, A. S., Mullenbach, B. L., Nittrouer, C. A., Parsons, J. D., and Sternberg, R. W.:
731 Storm-induced sediment gravity flows at the head of the Eel submarine canyon, northern California
732 margin, *Journal of Geophysical Research: Oceans*, 109, C03019, 2004.
- 733 Renssen, H., Seppa, H., Heiri, O., Roche, D. M., Goosse, H., and Fichet, T.: The spatial and
734 temporal complexity of the Holocene thermal maximum, *Nature Geosci*, 2, 411-414, 2009.
- 735 Richter, T. O., van der Gaast, S., Koster, B., Vaars, A., Gieles, R., de Stigter, H. C., De Haas, H., and
736 van Weering, T. C. E.: The Avaatech XRF Core Scanner: technical description and applications to
737 NE Atlantic sediments, Geological Society, London, Special Publications, 267, 39-50, 2006.
- 738 Roberts, N., Brayshaw, D., Kuzucuoğlu, C., Perez, R., and Sadori, L.: The mid-Holocene climatic
739 transition in the Mediterranean: Causes and consequences, *The Holocene*, 21, 3-13, 2011a.
- 740 Roberts, N., Eastwood, W. J., Kuzucuoğlu, C., Fiorentino, G., and Caracuta, V.: Climatic, vegetation
741 and cultural change in the eastern Mediterranean during the mid-Holocene environmental
742 transition, *The Holocene*, 21, 147-162, 2011b.
- 743 Rogerson, M., Schönfeld, J., and Leng, M. J.: Qualitative and quantitative approaches in
744 palaeohydrography: A case study from core-top parameters in the Gulf of Cadiz, *Marine Geology*,
745 280, 150-167, 2011.
- 746 Schimmelpfennig, I., Schaefer, J. M., Akçar, N., Ivy-Ochs, S., Finkel, R. C., and Schlüchter, C.:
747 Holocene glacier culminations in the Western Alps and their hemispheric relevance, *Geology*, 40,
748 891-894, 2012.
- 749 Schmiidl, G., Pfeilsticker, M., Hemleben, C., and Mackensen, A.: Environmental and biological
750 effects on the stable isotope composition of recent deep-sea benthic foraminifera from the western
751 Mediterranean Sea, *Marine Micropaleontology*, 51, 129-152, 2004.
- 752 Skonieczny, C., Paillou, P., Bory, A., Bayon, G., Biscara, L., Crosta, X., Eynaud, F., Malaize, B.,
753 Revel, M., Aleman, N., Barusseau, J. P., Vernet, R., Lopez, S., and Grousset, F.: African humid
754 periods triggered the reactivation of a large river system in Western Sahara, *Nat Commun*, 6, 2015.
- 755 Stanley, D. J. and Warne, A. G.: Worldwide Initiation of Holocene Marine Deltas by Deceleration of
756 Sea-Level Rise, *Science*, 265, 228-231, 1994.
- 757 Stuiver, M. and Reimer, P. J.: Extended 14C database and revised CALIB radiocarbon calibration
758 program, *Radiocarbon*, 35, 215-230, 1993.
- 759 Stuiver, M., Reimer, P. J., Bard, E., Beck, J. W., Burr, G. S., Hughen, K. A., Kromer, B., McCormac,
760 G., van der Plicht, J., and Spurk, M.: INTCAL98 radiocarbon age calibration, 24,000-0 cal BP,
761 2006.
- 762 Swindles, G. T., Plunkett, G., and Roe, H. M.: A delayed climatic response to solar forcing at 2800
763 cal. BP: multiproxy evidence from three Irish peatlands, *The Holocene*, 17, 177-182, 2007.
- 764 Thornes, J., Lopéz-Bermúdez, F., and Woodward, J.: Hydrology, river regimes and sediment yield. In:
765 *The physical geography of the Mediterranean*, J., W. (Ed.), Oxford University Press, Oxford, 2009.
- 766 Tornqvist, T. E. and Hijma, M. P.: Links between early Holocene ice-sheet decay, sea-level rise and
767 abrupt climate change, *Nature Geosci*, 5, 601-606, 2012.
- 768 Trigo, I. F., Davies, T. D., and Bigg, G. R.: Decline in Mediterranean rainfall caused by weakening of
769 Mediterranean cyclones, *Geophysical Research Letters*, 27, 2913-2916, 2000.
- 770 Ullman, D. J., Carlson, A. E., Anslow, F. S., LeGrande, A. N., and Licciardi, J. M.: Laurentide ice-
771 sheet instability during the last deglaciation, *Nature Geosci*, 8, 534-537, 2015.
- 772 Ulses, C., Estournel, C., Durrieu de Madron, X., and Palanques, A.: Suspended sediment transport in
773 the Gulf of Lions (NW Mediterranean): Impact of extreme storms and floods, *Continental Shelf*
774 *Research*, 28, 2048-2070, 2008.
- 775 van der Leeuw, S. E.: Climate, hydrology, land use, and environmental degradation in the lower
776 Rhone Valley during the Roman period, *Comptes Rendus Geoscience*, 337, 9-27, 2005.
- 777 Van der Zwaan, G. J., Duijnste, I. A. P., den Dulk, M., Ernst, S. R., Jannink, N. T., and
778 Kouwenhoven, T. J.: Benthic foraminifers: proxies or problems?: A review of paleocological
779 concepts, *Earth-Science Reviews*, 46, 213-236, 1999.
- 780 Vella, C. and Provansal, M.: Relative sea-level rise and neotectonic events during the last 6500yr on
781 the southern eastern Rhône delta, France, *Marine Geology*, 170, 27-39, 2000.
- 782 Walker, M. J. C., Berkelhammer, M., Björck, S., Cwynar, L. C., Fisher, D. A., Long, A. J., Lowe, J. J.,
783 Newnham, R. M., Rasmussen, S. O., and Weiss, H.: Formal subdivision of the Holocene
784 Series/Epoch: a Discussion Paper by a Working Group of INTIMATE (Integration of ice-core,



- 785 marine and terrestrial records) and the Subcommittee on Quaternary Stratigraphy (International
786 Commission on Stratigraphy), *Journal of Quaternary Science*, 27, 649-659, 2012.
- 787 Wanner, H., Beer, J., Bütikofer, J., Crowley, T. J., Cubasch, U., Flückiger, J., Goosse, H., Grosjean,
788 M., Joos, F., Kaplan, J. O., Küttel, M., Müller, S. A., Prentice, I. C., Solomina, O., Stocker, T. F.,
789 Tarasov, P., Wagner, M., and Widmann, M.: Mid- to Late Holocene climate change: an overview,
790 *Quaternary Science Reviews*, 27, 1791-1828, 2008.
- 791 Wanner, H., Mercolli, L., Grosjean, M., and Ritz, S. P.: Holocene climate variability and change; a
792 data-based review, *Journal of the Geological Society*, doi: 10.1144/jgs2013-101, 2014. 2014.
- 793 Wanner, H., Solomina, O., Grosjean, M., Ritz, S. P., and Jetel, M.: Structure and origin of Holocene
794 cold events, *Quaternary Science Reviews*, 30, 3109-3123, 2011.
- 795 Weaver, C. E.: Potassium, illite and the ocean, *Geochimica et Cosmochimica Acta*, 31, 2181-2196,
796 1967.
- 797 Weiss, B.: The decline of Late Bronze Age civilization as a possible response to climatic change,
798 *Climatic Change*, 4, 173-198, 1982.
- 799 Wirth, S. B., Glur, L., Gilli, A., and Anselmetti, F. S.: Holocene flood frequency across the Central
800 Alps – solar forcing and evidence for variations in North Atlantic atmospheric circulation,
801 *Quaternary Science Reviews*, 80, 112-128, 2013.
- 802 Zanchetta, G., Drysdale, R. N., Hellstrom, J. C., Fallick, A. E., Isola, I., Gagan, M. K., and Pareschi,
803 M. T.: Enhanced rainfall in the Western Mediterranean during deposition of sapropel S1:
804 stalagmite evidence from Corchia cave (Central Italy), *Quaternary Science Reviews*, 26, 279-286,
805 2007.
- 806 Zhornyak, L. V., Zanchetta, G., Drysdale, R. N., Hellstrom, J. C., Isola, I., Regattieri, E., Piccini, L.,
807 Baneschi, I., and Couchoud, I.: Stratigraphic evidence for a “pluvial phase” between ca 8200–
808 7100 ka from Renella cave (Central Italy), *Quaternary Science Reviews*, 30, 409-417, 2011.
- 809
- 810



811

812 **Tables**

813 Table 1: Chronology of Holocene cold relapses (CR) based on existing literature.

Event	Time slice (ky)	References
CR0	8.2	(Barber et al., 1999)
CR1	6.4-6.2	(Wanner et al., 2011)
CR2	5.3-5.0	(Magny and Haas, 2004; Roberts et al., 2011a)
CR3	4.2-3.9	(Walker et al., 2012)
CR4	2.8-3.1	(Chambers et al., 2007; Swindles et al., 2007)
CR5	1.45-1.65	(Wanner et al., 2011)
CR6	0.65-0.45	(Wanner et al., 2011)

814

815



816

817 Table 2: ^{14}C dates performed on core KSGC31

Depth (cm)	Material	Laboratory	Radiocarbon age $\pm 1\sigma$ error (yr BP)	Calibrated Age (cal BP)	$\pm 1\sigma$ error	Sedimentation Rate (SR) (mm/year)
5.5	<i>Bittium</i> sp.	Beta Analytics	420 \pm 30	24 ^a	60	-
11.5	<i>Tellina</i> sp.	Beta Analytics	430 \pm 30	34 ^a	60	-
18.5	<i>Pecten</i> sp.	Beta Analytics	720 \pm 40	350 ^b	78	-
25.5	<i>Venus</i> sp.	LMC14	640 \pm 30	234	99	1,34
41	<i>Pecten</i> sp.	LMC14	700 \pm 30	339	79	1,48
52	Indet. bivalve	LMC14	960 \pm 30	551	59	0,52
71	<i>Arca tetragona</i>	LMC14	1340 \pm 30	851	80	0,63
110.5	<i>Venus</i> sp.	LMC14	1465 \pm 30	992	85	2,80
186.5	<i>Nucula</i> sp.	LMC14	2235 \pm 40	1805	99	0,93
251	Juvenile bivalve shells (ind.)	LMC14	2940 \pm 30	2674	100	0,74
330.5	<i>Venus cosina</i>	LMC14	3870 \pm 30	3796	106	0,71
370.5	<i>Nuculana</i> sp.	LMC14	4170 \pm 30	4223	113	0,94
390.5	<i>Turritella</i> sp.	LMC14	4500 \pm 30	4676	106	0,44
460	<i>Venus</i> sp.	LMC14	5530 \pm 45	5873	106	0,58
481	<i>Ostrea</i> sp	LMC14	5955 \pm 35	6348	78	0,44
501.5	<i>Turritella</i> sp.	LMC14	6380 \pm 50	6826	107	0,43
552	Shells (mixed)	LMC14	7215 \pm 30	7653	75	0,61
583	<i>Turritella</i> sp.	LMC14	7860 \pm 60	8288	92	0,49
652	<i>Turritella</i> sp.	LMC14	8310 \pm 35	8843	121	1,24
700.5	<i>Turritella</i> sp.	LMC14	9215 \pm 30	10006	123	0,42
701	<i>Turritella</i> sp.	LMC14	9190 \pm 50	9968	145	-



818

819 Table 3: Timing of Holocene cold relapses (CRs; Jalali et al, this volume).

Cold relapses	Central Age year BP $\pm 1\sigma$ uncertainty	Age interval year BP	Duration year	Amplitude $^{\circ}\text{C}$
CR1	6175 \pm 133	6600 - 5750	850	1.3 \pm 0.3
CR2	5195 \pm 196	5350 - 5040	310	1.3 \pm 0.3
CR3	4130 \pm 126	4340 - 3920	420	2.4 \pm 0.3
CR4	2355 \pm 142	2530 - 2180	350	1.4 \pm 0.3
CR5	1365 \pm 119	1770 - 960	810	2 \pm 0.3
CR6	320 \pm 75	490 - 150	340	1.1 \pm 0.3

820

821

822 Table 4: Time uncertainty (1σ) of “wet spells” identified on the Ca/Ti and K/Ti ratios

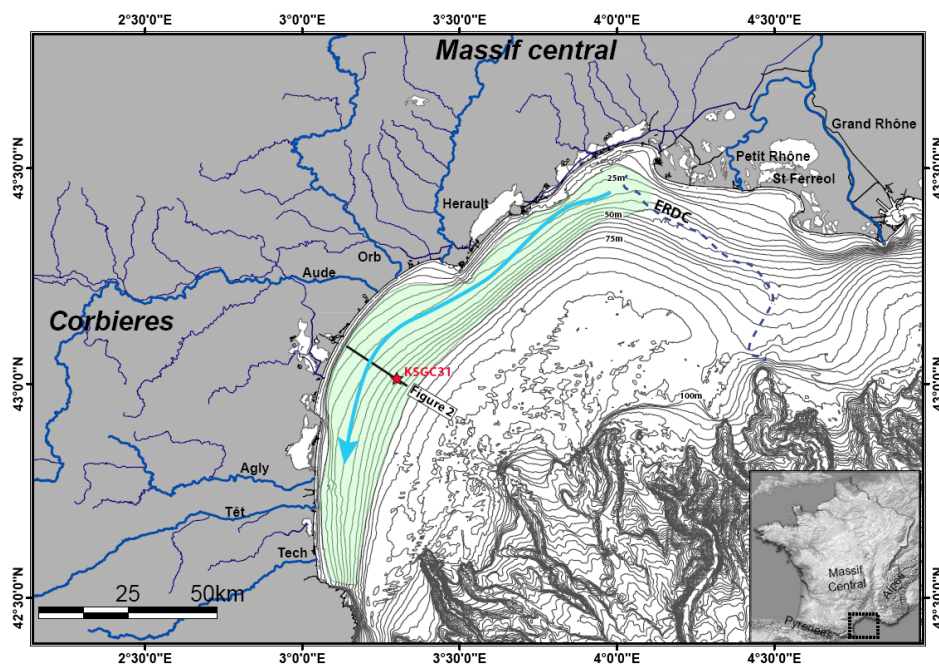
823 (Figure 4)

Abbreviation in the text	Start (yr cal BP)	Maximum (yr cal BP)	$\pm 1\sigma$ uncertainty	End (yr cal BP)	Proxy
0.72 ka	645	720	72	800	Ca/Ti
1.01 ka	1000	1015	75	1070	Ca/Ti
1.5 ka	1400	1500	124	1640	Ca/Ti
2.2 ka	2080	2200	145	2300	Ca/Ti
2.84 ka	2700	2840	172	2900	Ca/Ti
3.5 ka	3350	3500	170	3615	Ca/Ti
4.8 ka	4670	4800	150	4960	K/Ti
5.7 ka	5530	5700	162	5770	K/Ti

824

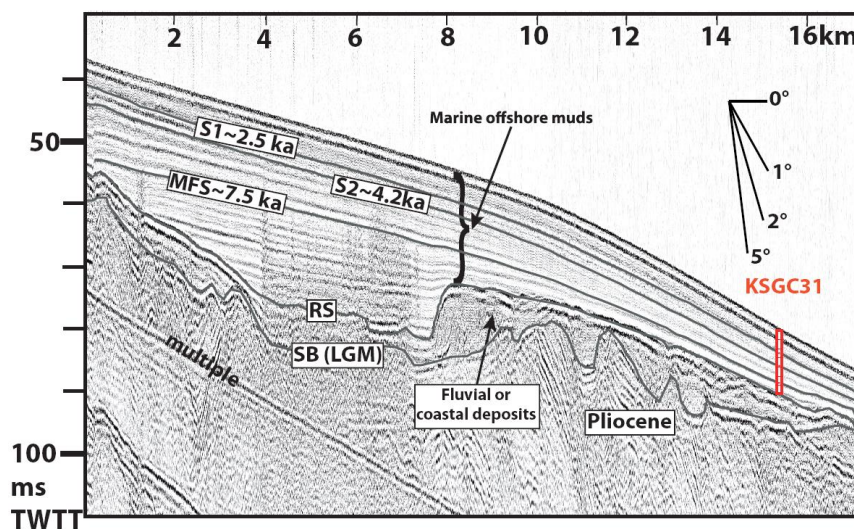


825



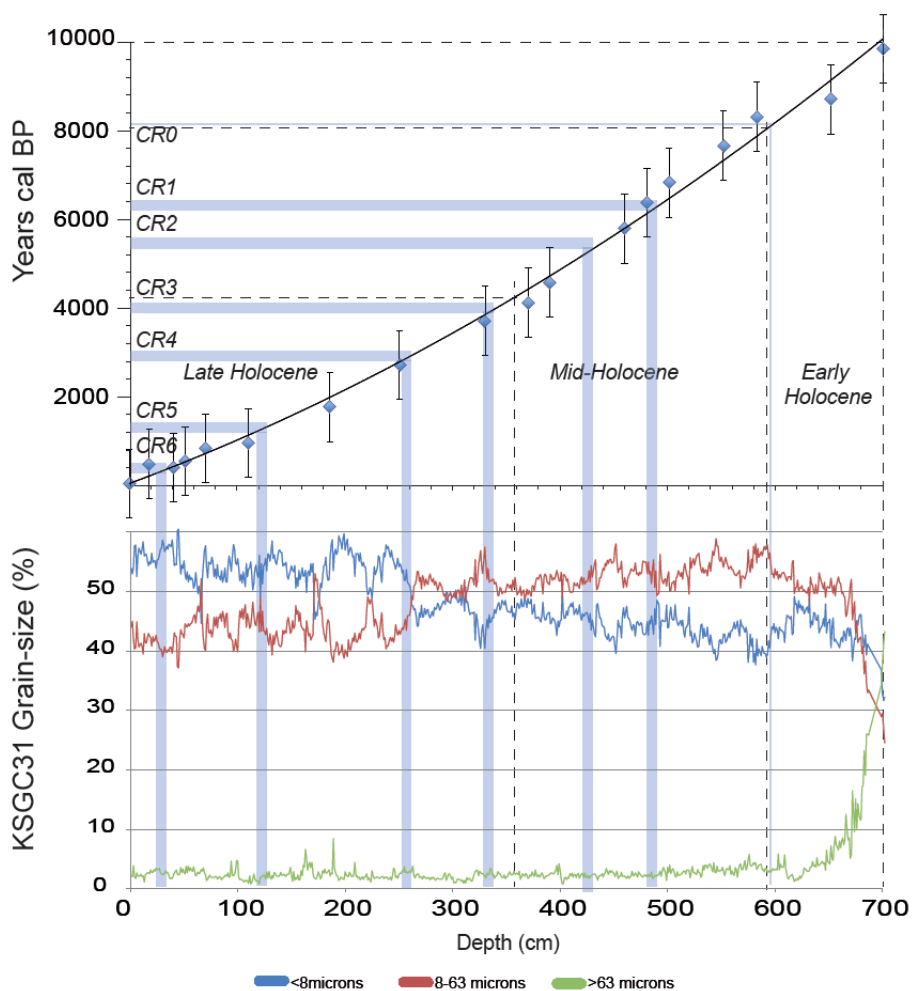
826

827 **Figure 1:** Bathymetric map of the Gulf of Lions and position of core KSGC31. The
828 approximate extent of the Rhone mud belt is represented in green; the arrow represents the
829 direction of dominant transport of suspended sediments . Bathymetric map based on Berné et
830 al. (2007). Contour lines every 5 m on the shelf. The dotted line corresponds to the retreat
831 path of the Rhone during the Deglacial (based on Gensous and Tesson, 2003; Berné et al.,
832 2007; Jouet, 2007; Fanget et al., 2014, Lombo Tombo et al., 2015). ERDC: Early Rhone
833 Deltaic Complex.



834

835 **Figure 2:** Seismic profile across the Rhone Mud Belt at the position of core KSGC31
836 (position in Figure 1). **SB:** Sequence Boundary- surface formed by continental erosion during
837 the Last Glacial Maximum (LGM). **RS:** *Ravinement* Surface formed by wave erosion during
838 sea-level rise. It corresponds to the coarse interval at the base of the core. **MFS :** Maximum
839 Flooding Surface (MFS). It corresponds to the phase of transition between coastal
840 retrogradation and coastal progradation. It is dated here at ca. 7.5 ka cal BP (i.e. the period of
841 global sea-level stabilization). S1 and S2 are seismic surfaces used as time lines (on the basis
842 of the age model in Figure 3 (respectively 4.2 ± 0.5 ka cal BP and 2.5 ± 0.5 ka cal BP).
843 Horizontal bars every meter along the core.



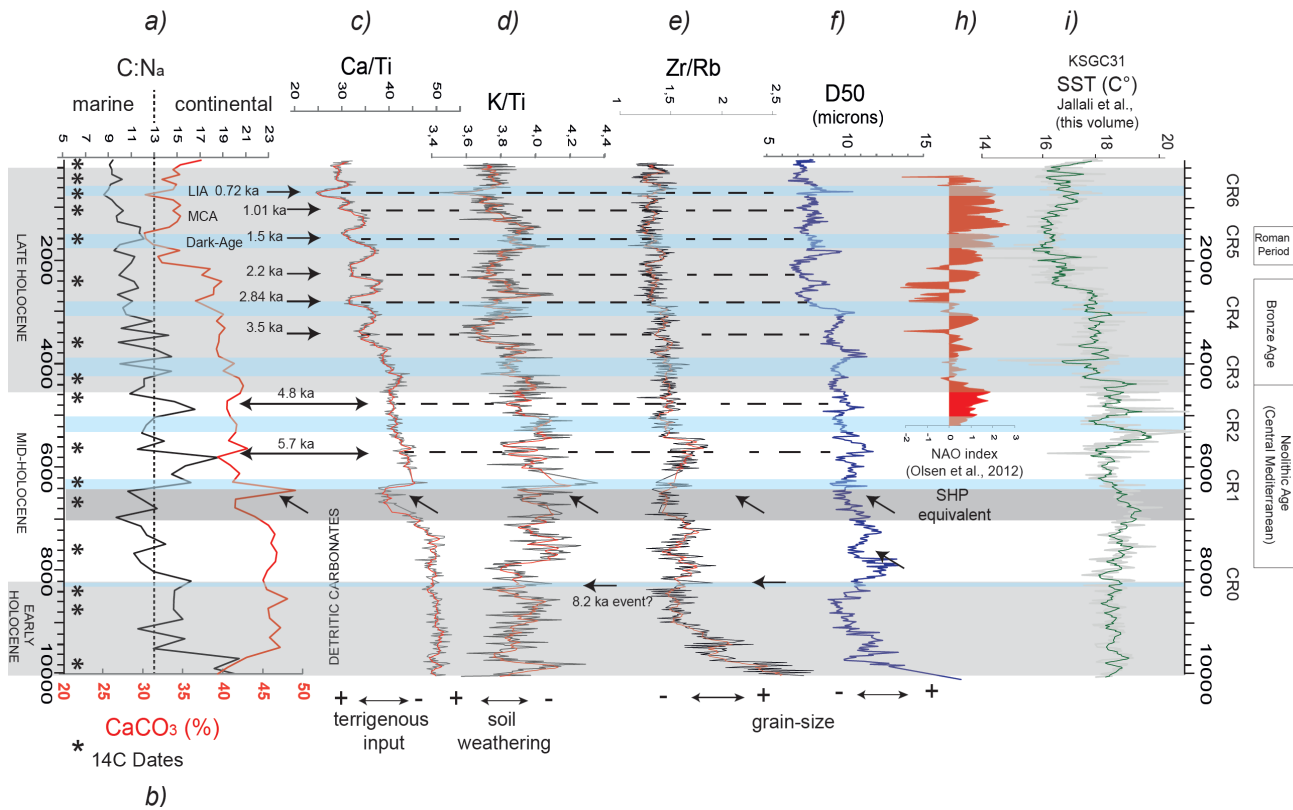
844

845 **Figure 3:** Correlation age-depth in core KSGC31. The Holocene time is divided into Early,
846 Middle and late Holocene according Walker et al. (2012). General core lithology is shown
847 through distribution of three grain-size classes: <8 μ m, 8-63 μ m, 63 μ m.

848

849

850

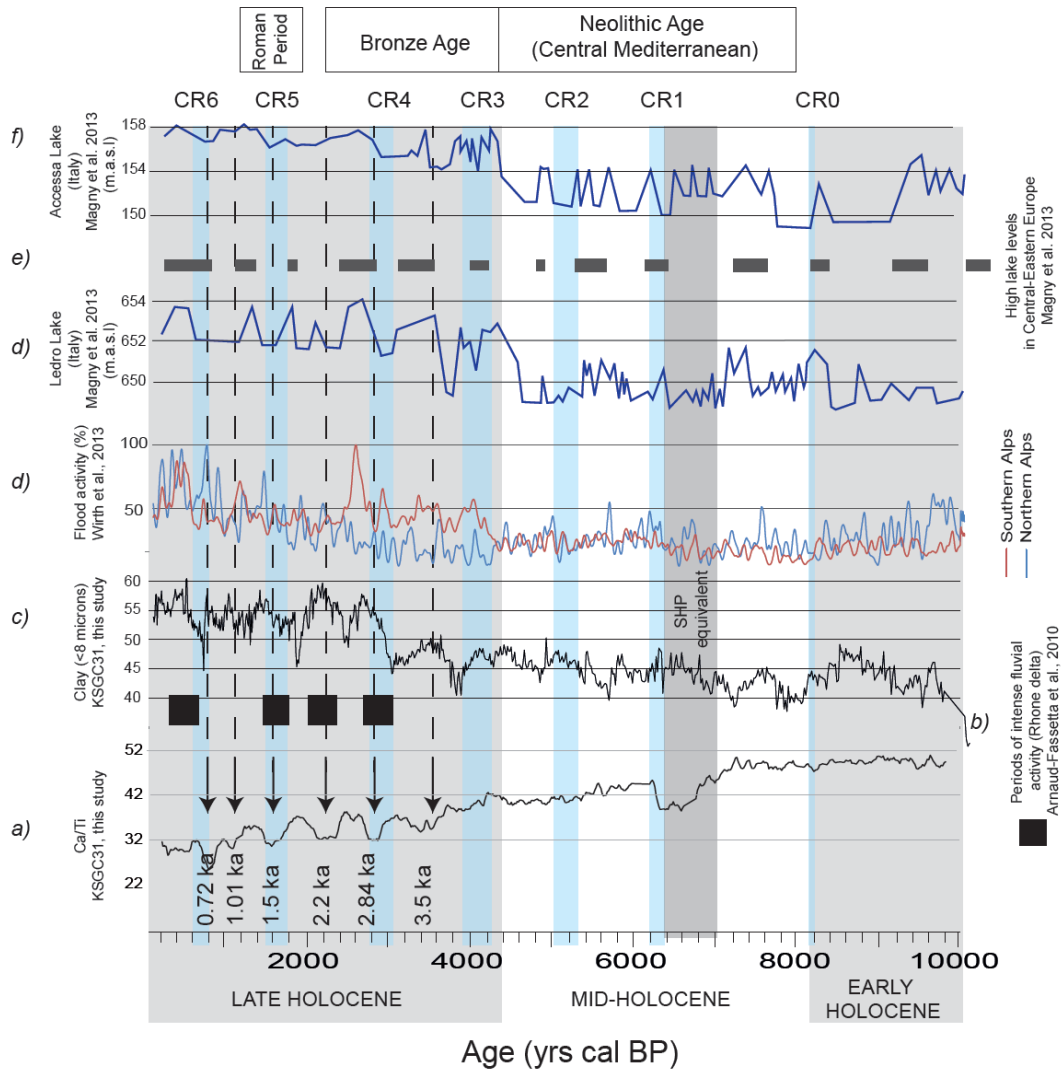




852 **Figure 4:** KSGC31 geochemical and sedimentological proxies: (a) C:N_a atomic ratio is used
853 as qualitative descriptor of organic matter nature. Values of C:N_a ratio > 13 indicate
854 significant amount of terrestrial organic matter, according to Goñi et al. (2003); (b) CaCO₃
855 content (%) calculated from TC-OC using the molecular mass ratio (CaCO₃: C= 100:12); (c)
856 Ca/Ti ratio is used for estimating the degree of detritism, since Ti is commonly found in
857 terrigenous sediments; (d) K/Ti ratio can be related to illite content, formed by weathering of
858 K-feldspars. Illite might be depleted in K upon pedogenetic processes, the K/Ti ratio can be
859 considered as an indirect proxy for the intensity of chemical weathering (Arnaud et al., 2012);
860 (e) Zr/Rb is known to reflect changes in grain size. Zr is commonly associated with the
861 relatively coarse-grained fraction of fine-grained sediments, whereas Rb is associated with
862 fine-grained fraction; (f) D50 represents the maximum diameter of 50% of the sediment grain
863 size. These plots are correlated to reconstruction of NAO (h) from a lake in Greenland (Olsen
864 et al., 2012) and reconstructed SST (C°) from alkenones (j) in core KSGC31 (Jalali et al., this
865 volume).



866



867

868 **Figure 5:** Ca/Ti ratio (a) and percentage of fine-grained (<8µm) sediment (c) compared to: b)
 869 Periods of intense fluvial activity based on hydromorphological and paleohydrological
 870 changes in the Rhone delta (Arnaud-Fassetta et al., 2010); d) Holocene flood frequency (%) in
 871 Southern and Northern Alps estimated on the basis on lake flood records by Wirth et al.
 872 (2013); e); f); g) lake level fluctuations in Central and Eastern Europe during the Holocene
 873 (Magny et al., 2013)